Materials and Design 50 (2013) 427–432

Contents lists available at SciVerse ScienceDirect

Materials and Design

journal homepage: www.elsevier.com/locate/matdes

Properties of high specific strength Al–4 wt.% Al_2O_3/B_4C nano-composite produced by accumulative roll bonding process

Morteza Alizadeh [a,*], Hossein Akbari beni [a], Mohammad Ghaffari [b], Rasool Amini [a]

[a] Department of Materials Science and Engineering, Shiraz University of Technology, Modarres Blvd., 71557-13944 Shiraz, Iran
[b] Department of Electrical and Electronics Engineering, UNAM-National Institute of Materials Science and Nanotechnology, Bilkent University, Ankara 06800, Turkey

ARTICLE INFO

Article history:
Received 8 January 2013
Accepted 8 March 2013
Available online 16 March 2013

Keywords:
Nano-composites
Metal-matrix composites
Mechanical properties
Transmission electron microscopy

ABSTRACT

The influence of nano-scale reinforcement on the mechanical and microstructural properties of ultrafine-grained composites was studied. Al matrix (pure aluminum) composites, with a grain size of 230 nm and B_4C and Al_2O_3 reinforcements with an average size of 50 nm, were fabricated via the accumulative roll bonding (ARB) process. To evaluate structure and microstructure of the produced composites, X-ray diffraction analysis (XRD) and transmission electron microscopy (TEM) were applied. Mechanical properties of the specimens were investigated by tensile and hardness tests. The result revealed that in comparison with monolithic Al (ARBed Al without ceramic particles), the presence of nano-particles enhances specific strength of composites. Also, the results showed that with increasing ARB cycles, the microhardness of the composites increases. In addition, the specific strength and microhardness of the composite samples are higher than those of the monolithic Al. The density of the composite samples and monolithic Al was measured by the Archimedes method showing that the density decreases in presence of ceramic particles.

1. Introduction

Aluminum alloys have many industrial applications due to their high specific strength and good corrosion resistance [1]. However, their mechanical properties such as elastic modulus, strength and wear resistance are not enough for industrial applications; therefore, they are reinforced by various methods. Although there are so many metallic alloy systems which can be used as a matrix, most attempts have been concentrated on Al alloys due to their low density, heat treatment capability, wide range of alloys and processing flexibility. Al alloys reinforced by ceramic particles have been widely developed in industry due to their high wear resistance, sufficient hardness, high specific strength and corrosion resistance [2]. Furthermore, physical properties and electrical conductivity can be affected by particle reinforcement [3]. SiC, Al_2O_3, TiC, TiB_2 and B_4C are usually used as ceramic reinforcement particles in metal matrix composites (MMCs) [4–6]. It is noticeable that properties of aluminum matrix composites are affected by reinforcement particle characteristics such as type, size and shape as well as particle distribution [7,8]. For instance, the mechanical strength can be improved considerably by the addition of Al_2O_3 particles to the Al–matrix. Also, the presence of B_4C particles in the Al–matrix increases the thermal stability [4,5,9]. In addition, boron carbide is the third hardest technical material after diamond and cubic boron nitride at room temperature and it possesses an excellent hardness, outstanding elastic modulus, a low specific gravity, high wear resistance and high melting point therefore, it is an appropriate reinforcement in some metal matrix composites [10].

Recently, some severe plastic deformation (SPD) methods such as equal channel angular pressing (ECAP) [11–13], high pressure torsion (HPT) [13] and ARB [14–16] have been used to produce a nano-structured Al matrix composite with high strength. Among these methods, the ARB process is an available method for production of MMCs in the form of sheets. This process was used for the first time by present authors for production of nano-structured Al–SiC composites in 2008 [17]. In this process, after every rolling cycle, a specific strain is introduced into specimen. The amount of this strain is calculated by following equation [13]:

$$\varepsilon = n\frac{2}{\sqrt{3}}\ln\left(\frac{t_0}{t}\right) \quad (1)$$

where t_0 is the initial thickness of the stacked sheets, t the thickness after roll-bonding, and n the number of cycles.

By repeating this procedure, very high strains are introduced successfully into specimens, and as a result, significant structural refinement is achieved [18]. In addition to structural refinement, by increasing the rolling cycles, the reinforcement particles begin to distribute in the Al matrix and by the final ARB cycles, the

* Corresponding author. Tel.: +98 711 7278491; fax: +98 711 7354520.
E-mail address: Alizadeh@sutech.ac.ir (M. Alizadeh).

0261-3069/$ - see front matter © 2013 Elsevier Ltd. All rights reserved.
http://dx.doi.org/10.1016/j.matdes.2013.03.018

particles are well distributed [17]. The aim of this research is to produce Al/Al_2O_3–B_4C nano-composite and nano-structured monolithic Al using the ARB process and to evaluate the microstructure and mechanical properties of the produced materials.

2. Experimental details

2.1. Materials

As-received commercial purity aluminum (AA 1050) sheets were cut into 200 mm × 40 mm × 0.5 mm pieces parallel to the sheet rolling direction. Al_2O_3 and B_4C particles (with an average size of 50 nm) were used as reinforcement.

2.2. Sample preparation

Strips of commercial purity aluminum were annealed at 623 K at ambient atmosphere. The strips were degreased in acetone and scratch brushed with a 90 mm diameter stainless steel circumferential brush with 0.35 mm wire diameter and surface speed of 14 m s^{-1}. To fabricate the composites by the ARB process, four strips were stacked over each other to achieve a 2 mm thickness, while about 1.35 wt.% Al_2O_3 and B_4C powders were dispersed between each of the two layers (Fig. 1a). The stacked strips were fastened at both ends with steel wire to prepare it for the rolling process. The strips were roll-bonded with a draft percentage of 50% reduction (von Mises equivalent strain of 0.8) in one cycle at room temperature (first step). At this cycle which was named the first cycle, the number of Al_2O_3–B_4C layers was three and the number of aluminum layers was 4. In the next step, the roll-bonded strip was cut into two strips by a shearing machine and degreased in acetone, scratch brushed and after stacking over each other, without Al_2O_3–B_4C particles between them, roll-bonded with a draft percentage of 50% reduction again. The last step of the process (second step) was repeated up to nine cycles without annealing between each cycle (Fig. 1b). After nine cycles, the Al matrix composite, including the well dispersed Al_2O_3–B_4C reinforcements, was produced. The ARB experiments were carried out, without lubricant, using a laboratory rolling mill with a load capacity of 20 tons. The roll diameter was 230 mm, and the rolling speed (ω) was 15 rpm (133.44 mm s^{-1}).

2.3. Microstructural evaluation

Microstructural observations were performed using an optical and transmission electron microscope (Philips-FEG). The TEM samples after the ARB process were prepared using electrolytical thinning in an electrolyte consisting of 1/3 HNO_3 and 2/3 CH_3OH at subzero temperatures. Thin foils parallel to the rolling plane (rolling direction–transverse direction or RD–TD plane) were prepared by the ion milling technique.

The XRD measurements were carried out on the RD–TD plane of the ARB processed sheets. The XRD experiment was performed by an X-ray diffractometer (XRD, Bruker Advance 2) using Cu $K\alpha_1$ radiation (λ = 0.15406 nm). The data was collected at room temperature with a 2θ range between 20° and 100° with a step size and scan rate of 0.03° and 6 s, respectively. The X-ray tube was operated at 40 kV and 40 mA. In the present study, Rietveld refinement of XRD patterns was done using MAUD software (by Luca Lutterotti, 1997–2011, University of Trento-Italy) and the required structural and microstructural information of the individual phases was then extracted.

2.4. Mechanical properties

Mechanical properties of the composites were determined by micro-hardness and uniaxial tensile tests. The tensile test samples were machined from the ARBed strips oriented along the rolling direction, according to the 1/5 scale of the JIS-No. 5. The gauge width and length of the tensile test samples were 5 and 10 mm, respectively and the length of them was 50 mm. The tensile tests were conducted at ambient temperature on an Instron testing machine at an initial strain rate of 8.3 × 10^{-4} s^{-1}. To have accurate results, at least five tensile experiments were conducted on each

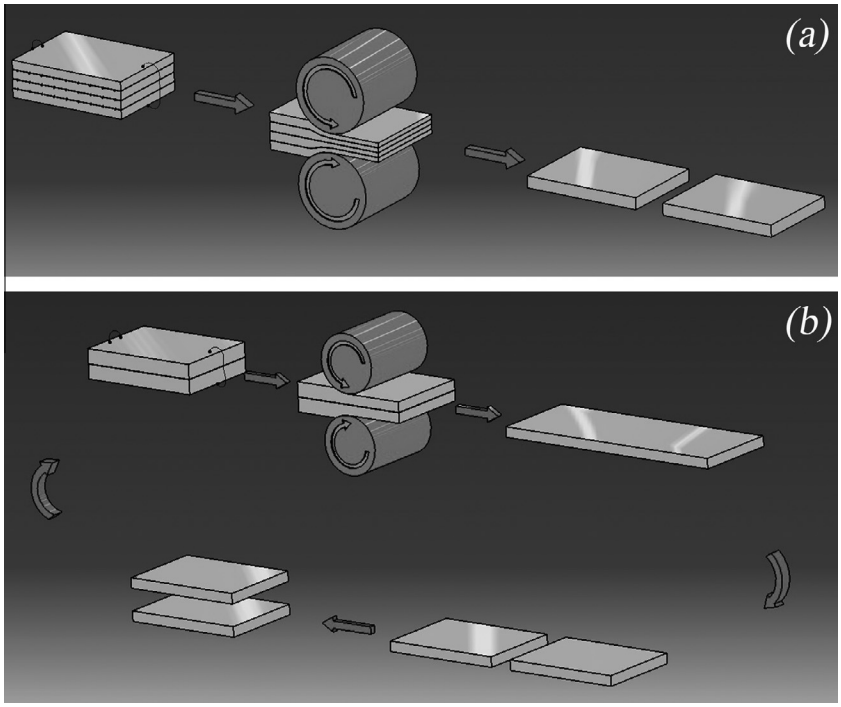

Fig. 1. Schematic illustration of the production process of the Al/ Al_2O_3–B_4C nano-composite sheets through the ARB process: the first step (a) and the second step (b).

sample and subsequently averaged. The total elongation of the specimens was determined as the difference between gauge lengths before and after testing.

Vickers microhardness (HV) tests, using a load of 15 g for 15 s (according to ASTM: E 384 standard), were performed on the cross-section (TD plane) of the ARB processed samples. The length, width, and thickness of the hardness test samples were 10, 10 and 1 mm, respectively.

The mean value of ten separate measurements taken at randomly selected points on the composite was reported.

2.5. Density test

The density of the specimens was measured by the Archimedes water immersion method (according to ISO 2738 standard) [19]. The theoretical density of the composites was calculated. The density of the pure Al, B_4C and Al_2O_3 powders was supposed to be 2.6989, and 2.52, 3.97 g/cm^3, respectively.

3. Results and discussion

The XRD pattern of Al–Al_2O_3–B_4C nano-composite produced by the ARB process after nine cycles (Fig. 2) shows that only Al, Al_2O_3 and B_4C phases are present in this composite and there is no new phase in the XRD pattern. Since the ARB process is performed at room temperature, the chemical reaction between the present elements does not occur. During the ARB process, due to friction between strips and rolls, the temperature increases, however, it is negligible for chemical reaction. It has been reported that during the ARB process the specimen temperature is increased from room temperature to about 100 °C [20] whereas, the required temperature for reaction is higher than this. For example B_4C can react with Al_2O_3 at 1900 °C [21].

The XRD results show that the percentage of Al_2O_3 particles in the composite increases in amount from the originally added Al_2O_3 particles in the first ARB cycle. This is attributed to aluminum oxides which are formed on the surface of the strips after wire brushing and before the rolling process. It has been reported that during specimen preparation, a layer of oxide film is formed on each surface of specimen [20]. These oxide films are fragmented during rolling process due to rolling pressure and are introduced into the specimen. Since there are a large number of free surfaces in this process, a large amount of oxide film is formed during the rolling process. After fragmentation, a considerable amount of Al_2O_3 particles are introduced into specimen. For instance, as mentioned in the experimental section in the first ARB cycle four strips are used which introduces six interfaces. Therefore, in the first ARB cycle six oxide layers are created and introduced into ARBed specimen. After several cycles of the ARB process, a large number of interfaces and consequently a large number of oxide films are introduced into the specimen. As a result, due to the formation of aluminum oxide on the treated surfaces, the percentage of Al_2O_3 particles in the composite specimens are a little greater than the Al_2O_3 particles that were added initially.

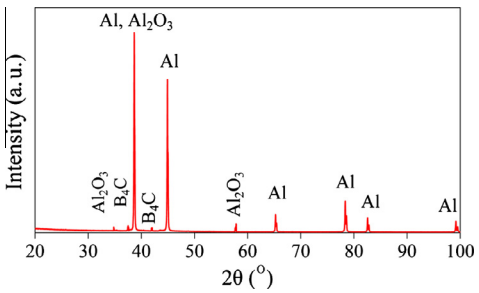

Fig. 2. XRD pattern of the Al/Al_2O_3–B_4C nano-composite processed by nine ARB cycles.

Fig. 3a and b presents a TEM image of the B_4C and Al_2O_3 nano-particles respectively. The nano-particles have a uniform distribution. The TEM microstructure and corresponding selected area diffraction pattern of the Al/Al_2O_3–B_4C nano-composite after nine ARB cycles has been shown in Fig. 4. As can be seen, the reinforcement particles have been homogeneously distributed into the Al matrix. Reinforcement distribution in the matrix is one of the effective parameters in the composite properties. The non-uniformity in the reinforcement arrangement can have significant effects on the mechanical properties of the composites. For example, it has been reported that yield strength and work hardening increases with increased clustering whereas the failure strain is significantly reduced in a clustered microstructure [22]. This is often attributed to the stress concentration in the particle clusters [23], which may lead to preferential nucleation and propagation of damage in the clusters.

It is noticeable that due to high activity and proneness to agglomeration of nano-particles, one major challenge to manufacture nano-composites is how the reinforcing particles disperse homogenously throughout the matrix. One way to improve particle distribution in the matrix is by using the ARB process in production of nano-composites. In the ARB process, by increasing the number of cycles, the ceramic particles are distributed in two directions: the normal direction (ND) and the rolling direction (RD). By progression of ARB, the number of Al and ceramic layers is increased and the ceramic particles are distributed in the ND. For example, after the first ARB cycle the number of Al and reinforcement layers is 4 and 3 respectively, whereas they reached to 1024 and 768 layers after nine ARB cycles respectively. The distance between two

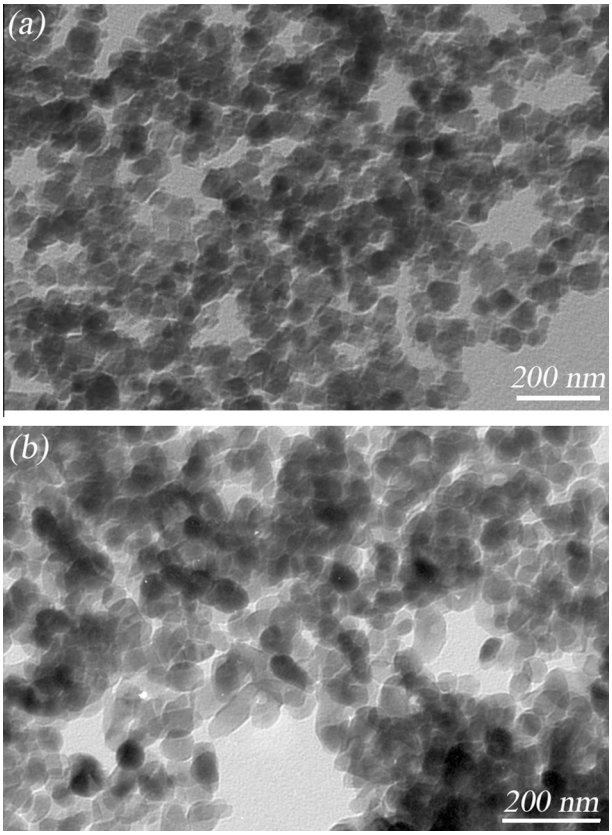

Fig. 3. TEM micrograph of (a) B_4C and (b) Al_2O_3 particles.

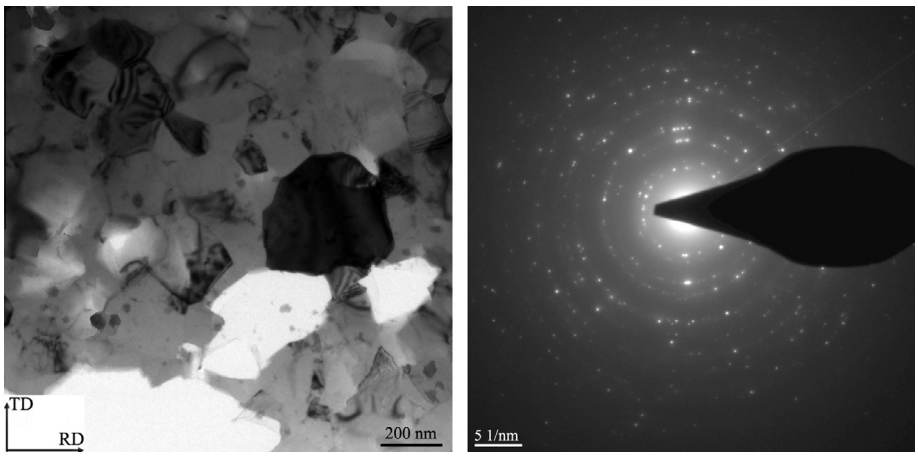

Fig. 4. TEM microstructure and associated selected area diffraction (SAD) pattern of the Al/Al_2O_3–B_4C nano-composite in ninth cycles.

reinforcement layers after the first ARB cycle is 250 μm and it is about 0.9766 μm after nine ARB cycles. This shows that the reinforcement particles are distributed in the Al matrix in the normal direction. In addition, under the normal roll pressure, the matrix material is extruded and flows through reinforcement particle clusters. As a result, dense particle clusters (agglomerated reinforcement particles) can be converted to diffuse clusters, and the distance between the particles constituting the clusters is enhanced, this means there is dissociation of the clusters and the development of the reinforcement distribution. In addition, since during the ARB process the Al strips are elongated in the RD, particle clusters are also elongated in the RD due to the strip elongation. This promotes the cluster expansion and the transition of dense-to-diffuse clusters, as accompanied by the matrix infusion between the particles. Therefore, due to the decrease of the Al layer thickness and elongation during the ARB process: (a) the distance between cluster particles is increased, (b) clusters are dissociated, and (c) particle-free zones are contracted. These events cause to number of dense particle clusters and diffuse clusters to decrease and cause the particles to disperse homogenously throughout the matrix. It should be noted that the dense particle clusters are denominated as particle agglomerations where no matrix material is present between the particles, while particle clusters with some amount of the matrix material between the particles are denominated as diffuse clusters [24]. Fig. 5 shows the TEM microstructure of the Al/Al_2O_3–B_4C nano-composite after four ARB cycles which consists of a particle agglomeration. It is noticeable that this particle agglomeration is eliminated in higher numbers of cycles.

Fig. 4 shows that after nine ARB cycles, an ultra-fine grained matrix with an average size of 230 nm is present in the specimen. Tsuji et al. suggested that the formation mechanism of these ultra-fine grains in the ARB process is grain subdivision [15]. In the initial ARB cycles, due to applied strain, dislocations are produced, their density is increased and dislocation cell structure is created [25]. In the intermediate ARB cycles the dislocation density in cells decreases and the cell size become fine. Ultra-fine grains and sub-grains are also created in the specimen during these cycles [25]. In the final cycles the ultra-fine grains are completely developed in the specimen [25].

In both the composite specimen (regardless of the ceramic particles) and monolithic Al specimen, hardness is increased with increasing number of ARB cycles. This is attributed to strengthening mechanisms which are activated during the ARB process, such as strain hardening (based on the density of dislocations and interaction between them) and grain refinement [26]. It is noticeable that the hardness of metals increases proportionally to the minus

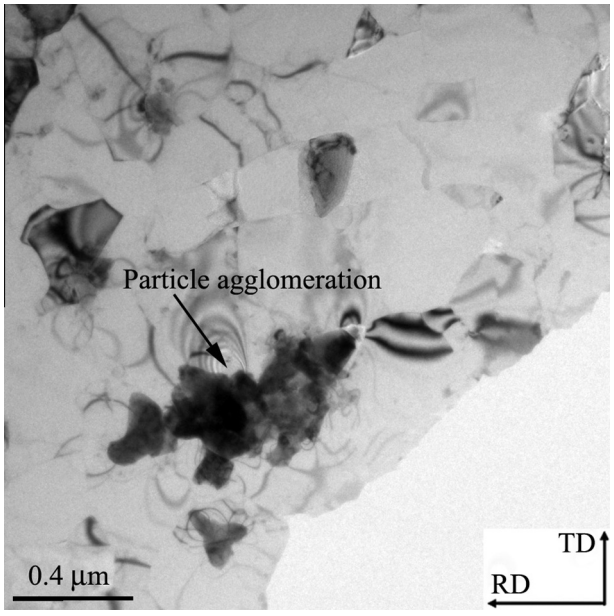

Fig. 5. TEM microstructure of the Al/Al_2O_3–B_4C nano-composite in fourth cycles.

square root of the grain size ($d^{-1/2}$), which is called the Hall–Petch relationship.

It has been reported that strain hardening which occurs in the initial ARB cycles, has more effect on increasing microhardness than the grain refinement [27]. For example, as is seen in Fig. 6,

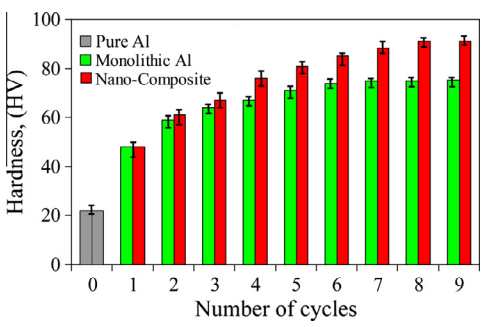

Fig. 6. Variation of microhardness vs. the number of the ARB cycle in the ARBed nano-composite and monolithic samples.

there is an immediate increase in microhardness by a factor of approximately 2.5 at a strain of 0.8 (first cycle). In the intermediate ARB cycles, the microhardness growing rate is relatively low, since the contribution of the strain hardening on the microhardness increasing is considerably reduced. According to the literature [26], in these cycles, the increase of microhardness has been attributed to the grain refinement. In the final ARB cycles, since materials reach the steady-state density of dislocation, the increase in microhardness stops and it remains at a steady-state value [26].

The presence of the ceramics nano-particles in the Al matrix during the ARB process affects the existing strengthening mechanisms and can also activate other strengthening mechanisms such as the Orowan strengthening mechanism in the matrix. For instance, during the ARB process, the ceramic particles increase dislocation density in the interface particles and the Al matrix due to the following reasons: (a) strain incompatibility between aluminum and ceramic particles, (b) difference in thermal expansion between aluminum and ceramic particles after the ARB process and during cooling [28–30]. As a result, grain refining is accelerated and the grain size in the matrix becomes smaller than that in the unreinforced aluminum [30]. Therefore, the microhardness values in the $Al/Al_2O_3–B_4C$ composites after initial ARB cycles are higher than unreinforced aluminum. In addition, due to high hardness of ceramic particles (for B_4C about 2900–3580 ($kg\,mm^{-2}$)), the hardness of the composite is also increased [31].

Table 1 lists some mechanical and physical properties of the raw materials, monolithic Al, and $Al/Al_2O_3–B_4C$ nano-composite. As it can be seen form Table 1, the density of as received pure Al strips is more than that of monolithic Al and also the density of monolithic Al is more than that of the $Al/Al_2O_3–B_4C$ nano-composite. The difference between densities of these materials is attributed to the percentage of the porosity in them. The creation of the porosity is regarded from two viewpoints: the non adequate welding between aluminum strips, and the presence of ceramic particles and particle clusters between Al layers. In the ARB process, a wire brushing step is done before every cycle in order to create a hard and brittle layer. Fig. 7 shows a wire brushed surface with different magnifications. As it can be seen, there is some tearing and some striations along the wire brushing direction. The existence of a hard and brittle layer on the surface of the strips is essential for the creation of successful bonding in the ARB process. During the ARB process, the hard and brittle wire brushed surface of strips is joined together by atom-to-atom bonding [26,32]. In fact, two strips are welded to each other due to rolling pressure. The effective weld area (or weld efficiency) between the two strips depends on following parameters [32]: (a) the metal under consideration, (b) the amount of deformation, (c) the amount of contamination layers (such as oxides, grease, humidity, and dust particles) between the surfaces of two strips, (d) the temperature of welding, (e) the metal purity, and (f) the surface preparation. These parameters should be at an optimum value to ensure appropriate bonding is created. However, in this study, the ARB process is performed at room temperature and 50% thickness reduction, the weld efficiency or weld area is not 100% (according to our previous study [33] it is about 65%) and therefore there is some porosity between the bonded strips. The presence of the mentioned porosity decreases the density of the ARBed samples in comparison with the pure aluminum. Furthermore, the presence of the ceramic particles can act as contamination on the surface of the strips and decrease the effective weld area between the two strips by inhibiting a successful bond between them; therefore, the percentage of porosity in the specimens is increased and consequently the density is decreased. In addition, there may be some particle agglomeration in the composite specimens during powder dispersing. It has been reported that there is porosity in the particle agglomerations which decreases the density of specimen [32,33]. As is seen from Table 1 the density of the $Al/Al_2O_3–B_4C$ nano-composite is lower than that of the ARBed pure Al (monolithic Al).

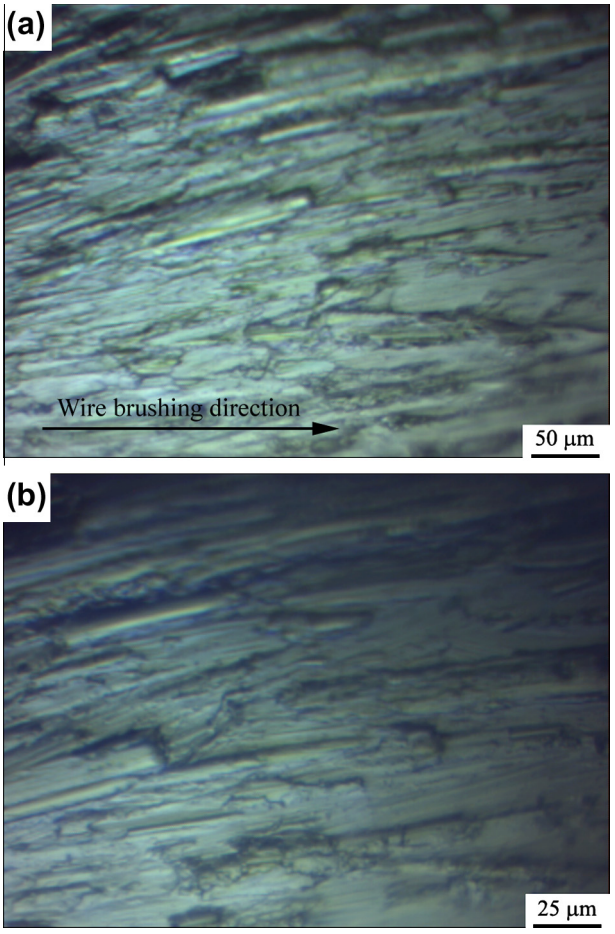

Fig. 7. OM micrograph of commercial pure aluminum after wire brushing and before ARB process with different magnifications.

The specific strength of the as received pure aluminum and ARBed specimens was calculated and compared. The specific strength is the material's strength (force per unit area at failure) divided by its density. Comparison of the specific strength of the as received pure aluminum with the monolithic Al and the $Al/Al_2O_3–B_4C$ nano-composite shows that, the ARB process increases the specific strength by a considerably amount. The specific strength of the ARB processed pure Al is about 3.4 times larger than that of the as received pure Al. As mentioned above, the specific strength of a material depends on its density and strength. It has been reported that in the ARB process, the strength is increased dramatically and sometimes it reaches about 3 times of the starting material due to dislocation strengthening and boundary

Table 1
Some properties of the raw materials, monolithic Al, and $Al/Al_2O_3–B_4C$ nano-composite.

Materials	Density (g/cm^3)	Strength (MPa)	Specific strength (N m/kg)
B_4C	2.52	-	-
Al_2O_3	3.97	-	-
Pure Al	2.6989	50	1.852×10^4
Monolithic Al	2.6131	165	6.314×10^4
$Al/B_4C–Al_2O_3$	2.5612	269	10.5×10^4

strengthening [31], which increases the specific strength. As is seen in Table 1, the strength and specific strength of the Al/Al_2O_3–B_4C nano-composite is higher than that of monolithic Al. This is attributed to the presence of reinforcement particles in the Al matrix during the ARB process.

4. Conclusion

In this study, Al/Al_2O_3–B_4C composites and monolithic Al were fabricated in the form of sheets via the ARB process. The microstructure and mechanical properties of these materials were investigated and compared. According to the results, it can be concluded that:

(1) The XRD results show that the Al/Al_2O_3–B_4C nano-composite was successfully produced via the ARB process without any additional phase.
(2) The microhardness of the composites and pure Al increased with increasing the amount of ARB cycles.
(3) The specific strength and microhardness of the composite samples are higher than those of the monolithic Al.
(4) The density of the ARB processed materials is lower than that of as received pure Al.
(5) The presence of ceramic particles in the Al matrix increases the porosity and consequently decreases the density.
(6) The ARB process is an available method for elimination of present nano-particle agglomerations in the matrix.
(7) A homogeneous distribution of nano-particles is achieved during the ARB process due to the increase of layers and elongation along the rolling direction.

References

[1] Rezaei MR, Toroghinejad MR, Ashrafizadeh F. Effects of ARB and ageing processes on mechanical properties and microstructure of 6061 aluminum alloy. J Mater Process Technol 2011;211:1184–90.
[2] Derakhshandeh Haghighi R, Jenabali Jahromi SA, Moresedgh A, Tabandeh Khorshid M. A Comparison between ECAP and conventional extrusion for consolidation of aluminum metal matrix composite. J Mater Eng Perform 2012;21:1885–92.
[3] Liu CY, Wang Q, Jia YZ, Zhang B, Jing R, Ma MZ, et al. Effect of W particles on the properties of accumulatively roll-bonded Al/W composites. Mater Sci Eng A 2012;547:120–4.
[4] Huber T, Degischer HP, Lefranc G, Schmitt T. Thermal expansion studies on aluminium–matrix composites with different reinforcement architecture of SiC particles. Comp Sci Technol 2006;66:2206–17.
[5] Tabandeh Khorshid M, Jenabali Jahromi SA, Moshksar MM. Mechanical properties of tri-modal Al matrix composites reinforced by nano-and submicron-sized Al_2O_3 particulates developed by wet attrition milling and hot extrusion. Mater Des 2010;31:3880–4.
[6] Yazdani A, Salahinejad E. Evolution of reinforcement distribution in Al–B_4C composites during accumulative roll bonding. Mater Des 2011;32:3137–42.
[7] Schmidt CW, Knieke C, Maier V, Hoppel HW, Peukertb W, Gokena M. Accelerated grain refinement during accumulative roll bonding by nano-particle reinforcement. Scripta Mater 2011;64:245–8.
[8] Peng Z, Fu-guo L. Effect of particle characteristics on deformation of particle reinforced metal matrix composites. T Nonferr Metal Soc 2010;20(4):655–61.
[9] Jamaati R, Toroghinrjad MR. Application of ARB process for manufacturing high-strength, finely dispersed and highly uniform Cu/Al_2O_3 composite. Mater Sci Eng A 2010;527:4146–51.
[10] Chung DL. Composite Materials: Functional Materials for Modern Technologies. London: Springer; 2003.
[11] Segal VM. Materials processing by simple shear. Mater Sci Eng A 1995;197:157–64.
[12] Reihanian M, Ebrahimi R, Tsuji N, Moshksar MM. Analysis of the mechanical properties and deformation behavior of nano-structured commercially pure Al processed by equal channel angular pressing (ECAP). Mater Sci Eng A 2008;473:189–94.
[13] Azushima A, Kopp R, Korhonen A, Yang DY, Micari F, Lahoti GD, et al. Severe plastic deformation (SPD) processes for metals. CIRP Ann Manuf Technol 2008;57:716–35.
[14] Saito Y, Utsunomiya H, Tsuji N, Sakai T. Novel ultra-high straining process for bulk materials development of the accumulative roll-bonding (ARB) process. Acta Mater 1999;47:579–83.
[15] Saito Y, Tsuji N, Utsunomiya H, Sakai T, Hong RG. Ultra-fine grained bulk aluminum produced by accumulative roll-bonding (ARB) process. Scr Mater 1998;39:1221–7.
[16] Tsuji N, Saito Y, Utsunomiya H, Tanigawa S. Ultra-fine grained bulk steel produced by accumulative roll-bonding (ARB) process. Scr Mater 1999;40:795–800.
[17] Alizadeh M, Paydar MH. Study on the effect of presence of TiH_2 particles on the roll bonding behavior of aluminum alloy strips. Mater Des 2009;30:82–6.
[18] Huang X, Tsuji N, Hansen N, Minamino Y. Microstructural evolution during accumulative roll-bonding of commercial purity aluminum. Mater Sci Eng A 2003;340:265–71.
[19] ISO 2738, Sintered metal materials, excluding hard metals – Permeable sintered metal materials – Determination of density, oil content and open porosity. New York: American National Standards Institute; 1999.
[20] Jamaati R, Toroghinejad MR, Dutkiewicz J, Szpunar JA. Investigation of nano-structured Al/Al_2O_3 composite produced by accumulative roll bonding process. Mater Des 2012;35:37–42.
[21] Swarnakar AK, Huang SG, Van der Biest O, Vleugels J. Ultrafine Al_2O_3–B_4C composites consolidated by pulsed electric current sintering. J Alloys Compd 2010;499:200–5.
[22] Ganguly P, Poole WJ. Characterization of reinforcement distribution inhomogeneity in metal matrix composites. Mater Sci Eng A 2002;332:301–10.
[23] Xu XQ, Watt DF. A numerical analysis of the effects of reinforcement content on strength and ductility in Al(SiC)p MMCs. Acta Metall Mater 1996;44:4501–11.
[24] Yazdani A, Salahinejad E. Evolution of reinforcement distribution in Al–B_4C composites during accumulative roll bonding. Mater Des 2011;32:3137–42.
[25] Lee SH, Saito Y, Tsuji N, Utsunomiya H, Sakai T. Role of shear strain in ultragrain refinement by accumulative roll-bonding (ARB) process. Scripta Mater 2002;46:281–5.
[26] Eizadjou M, Danesh Manesh H, Janghorban K. Microstructure and mechanical properties of ultra-fine grains (UFGs) aluminum strips produced by ARB process. J Alloys Compd 2009;474:406–15.
[27] Alizadeh M. Comparison of nano-structured Al/B_4C composite produced by ARB and Al/B4C composite produced by RRB process. Mater Sci Eng A 2010;528:578–82.
[28] Alizadeh M, Paydar MH. Fabrication of nano-structure Al/SiC_P composite by accumulative roll-bonding (ARB) process. J Alloys Compd 2010;492(1–2):231–5.
[29] Alizadeh M. Strengthening mechanisms in particulate Al/B_4C composites produced by repeated roll bonding process. J Alloys Compd 2011;509:2243–7.
[30] Alizadeh M, Paydar MH, Trada D, Tsuji N. Effect of SiC particles on the microstructure evolution and mechanical properties of aluminum during ARB process. Mater Sci Eng A 2012;540:13–23.
[31] Sarikaya O, Anik S, Celik E, Okumus SC, Aslanlar S. Wear behaviour of plasma-sprayed AlSi/B_4C composite coatings. Mater Des 2007;28:2177–83.
[32] Alizadeh M. Effects of temperature and B_4C content on the bonding properties of roll-bonded aluminum strips. J Mater Sci 2012;47:4689–95.
[33] Yazdani A, Salahinejad E, Moradgholi J, Hosseini M. A new consideration on reinforcement distribution in the different planes of nano-structured metal matrix composite sheets prepared by accumulative roll bonding (ARB). J Alloys Compd 2011;509:9562–4.